Wavelet transform filtering of seismic data by semblance weighting

Victor Iliescu and Gary F. Margrave

ABSTRACT

The presence of noise in a nonstationary signal (i.e., whose frequency content varies with time) complicates the extraction of meaningful information from the signal. The classical Fourier domain of such a signal can only separate the noise from the useful signal energy if they have different frequency content. For nonstationary signals the windowed Fourier transform has been introduced to localize the signal in time. The windowing is accomplished by a weight function that places less emphasis near an interval's endpoints than in the middle. The short-time Fourier transform (STFT) thereby decomposes a signal into a time frequency plane. Nonstationary filtering can be done by prescribing weights that vary with time and frequency, which are applied to the decomposed data. An inverse STFT then reconstructs the filtered signal. Recently, the wavelet transform (WT) has been applied in diverse fields such as mathematics, quantum physics, engineering and geophysics. The WT decomposes a signal in a time-scale frame. The seismic data can be filtered using the WT in a form similar to time-frequency filtering techniques. This paper explores a method of filtering seismic data using the discrete wavelet transform (DWT) with filter weights in the wavelet domain using a time-domain semblance measure. The semblance coefficients, as a measure of multichannel coherence, serve to emphasise the signal in the wavelet coefficients of the decomposed trace. This method has been tested on a Blackfoot final stack where it appears to improve the resolution of the section.

INTRODUCTION

The time-variant filtering technique was implemented to suppress nonstationary noise bursts in seismic data. To compensate for the limitations of the classical Fourier transform, the STFT was first introduced (Cohen, 1995). The windowed Fourier transform is the most widely used method for studying nonstationary signals. The time-variant spectrum (TVS) is a decomposition of a signal onto a time-frequency matrix. The TVS(τ,f) (Schoepp, 1998) is calculated by taking the STFT:

$$TVS\ (\tau,f) = \int_{-\infty}^{\infty} s(t)h(t-\tau)e^{-i2\pi ft}\,dt \quad , \tag{1}$$

where $s(t)$ is the signal and $h(t-\tau)$ is a time-shifted window with τ the fixed time and t the running time. The window width and the window increment are important parameters in the TVS computation. The width of the time window is determined by a fixed positive constant. In all of the STFT methods, (depending on the windows used) computational complexities arise when either narrowing of the window is required for better localization or widening of the window is required to obtain a better spectral resolution (Chui, 1992). A whitening technique applied to the TVS of

data (a stacked section from the Blackfoot broad band survey) will be used in this test to equalize the Fourier spectrum and therefore, the resolution. In comparison, the WT distinguishes itself from the STFT in that it has a zoom-in and zoom-out capability. Unlike the STFT in which the length of the window is fixed, the WT localizes signals in a variable window determined by the scale parameter.

The WT is a relatively new signal analysis and processing approach. There are few applications of the wavelet transform in geophysical data processing. Some examples are: data compression (Donoho, Ergas and Villasenor, 1995), time frequency analysis, filtering and interpretation using frequency-time plots (Chakraborty and Okaya, 1994), and phase correction using the wavelet transform (Rodriguez and Mansar, 1997). The WT of a signal decaying in time depends on two variables: scale and time. The strength of the WT representation is the separation of the signal in different scale levels. The result of the wavelet decomposition consists of coefficients that are influenced by local events that can be potentially identified, analysed, and filtered. The WT was used to filter the stacked section by applying weights to the wavelet coefficients. The weights are based on semblance in t-x domain.

MATHEMATICAL BACKGROUND

The WT is, like the Fourier transform, an inner product between the signal and a set of basis functions. The expansion coefficients reflect the similarity between the signal and the elementary basis functions. The elementary functions are also called analysis functions. The result of the inner product represents the expansion coefficient and the set of all expansion coefficients represents the wavelet domain.

There are many types of wavelet transforms. The most important are the continuous wavelet transform (CWT) and the discrete wavelet transform (DWT).

The CWT

The CWT can be thought of as the inner product of the signal with the basis functions $\psi_{a,b}(t)$, (Daubechies, 1992) ($\psi(t)$ is called the mother wavelet).

$$\langle s(t), \psi_{ab}(t) \rangle = CWT_{(a,b)} = \frac{1}{\sqrt{|a|}} \int_{-\infty}^{\infty} s(t)\psi^*(t)dt \qquad (2)$$

In this expression, $\psi_{a,b}{}^*(t)$ is the complex conjugate of

$$\psi_{a,b}(t) = \frac{1}{\sqrt{|a|}} \psi(\frac{t-b}{a}), \qquad (3)$$

for $\psi(t)$ real, $\psi^* = \psi$.

The scale index, a, can be thought as the reciprocal of the frequency while b indicates time shifting (or translation). The normalizing constant $a^{-1/2}$ is chosen so that the total

energy of the wavelet in the time domain is equal to the energy in the frequency domain. The wavelet energy can be expressed in the form:

$$\left\|\psi_{(a,b)}\right\|^2 = \int_{-\infty}^{\infty}\left|\Psi(\omega)\right|^2 d\omega = \int_{-\infty}^{\infty}\left|\psi(t)\right|^2 dt \qquad (4)$$

where the $\|\psi_{a,b}\|$ represents the Euclidean norm. Equation (4) represents Parseval's theorem applied to the wavelet and states that the total energy should be the integral of $\left|\Psi(\omega)\right|^2$, (where $\Psi(\omega)$ is the Fourier spectrum of the wavelet) over all frequencies and should equal the total energy of the wavelet in the time domain. This property can be extended to the signal in the wavelet domain (Qian. and Chen., 1996):

$$\int_{-\infty}^{\infty}\left|s(t)\right|^2 = \frac{1}{C_\psi}\int_{-\infty}^{\infty}\int_{-\infty}^{\infty}\frac{\left|CWT_{(a,b)}\right|}{a^2}dadb \qquad (5)$$

where C_ψ should satisfy the admissibility condition given by:

$$C_\psi = \int_{-\infty}^{\infty}\frac{\left|\Psi(\omega)\right|^2}{\left|\omega\right|}d\omega < \infty \qquad (6)$$

This theorem states that the weighted energy of the wavelet transform of the signal is equal to the energy of the signal in the time domain. When a is small, which corresponds to small support length, the wavelet transform picks up higher frequency components. If the admissibility condition is not satisfied the reconstruction is not possible because the inverse wavelet transform will diverge.

The coefficients of the CWT measure the closeness of the signal to the wavelet at the current scale. If the signal has a major component of the frequency corresponding to the current scale, then the wavelet at the current scale will be similar or close to the signal at the particular location where this frequency component occurs. Therefore, the CWT coefficient computed at this point in the time scale plane will be a relatively large number. The definition of the CWT shows that the wavelet analysis is a measure of similarity between the basis functions (wavelets) and the signal itself. Here, the similarity is in the sense of similar frequency content (Qian and Chen, 1996).

The inverse transform of the CWT is given by :

$$s(t) = \frac{1}{\sqrt{C_\psi}}\int_{-\infty}^{\infty}\int_{-\infty}^{\infty}\frac{1}{\sqrt{a}}\psi(\frac{t-b}{a})\frac{1}{a^2}CWT_{(a,b)}dtda \qquad (7)$$

A perfect reconstruction of the signal is possible, but depends on the choice of the elementary function $\psi_{a,b}(t)$. The CWT is highly redundant and therefore is computationally time consuming. The DWT computes only those scales and

translations needed for a complete representation and reconstruction of the signal. For this reason, the DWT is more efficient and has been used in this experiment.

The DWT and multi-resolution analysis

In the discrete wavelet transform (DWT), the dilation parameter a and the translation parameter b take only selected discrete values. Besides the CWT, another way to introduce wavelets is through multi-resolution analysis (MRA) (Mallat, 1999). The concept of the MRA is the key to the construction of orthogonal wavelet bases and to the fast decomposition of a signal into frequency bands. If s(t) is a signal from a certain subspace $V_{-1} \in L^2$ (R), a decomposition is performed into a high and low-frequency part. The low-frequency part, $P_0 S$ (called the approximation coefficients) is obtained by an orthogonal projection into a smaller subspace $V_0 \subset V_{-1}$ which contains only the smoothed functions of V_{-1}. The orthogonal complement of V_0 in V_{-1} will be denoted by W_0. The projection of the signal s(t) into W_0 will be denoted by $Q_0 S$ (called the detail coefficients).

In this way we have s(t)= $P_0 S + Q_0 S$ ($V_{-1} = V_0 \oplus W_0$). The procedure can be repeated to decompose $P_0 S$ into a coarser level of approximation and detail and so on. The result is an MRA of L^2 (R) (the space of finite energy functions) defined as a sequence of closed subspaces V_k of L^2 (R), k $\in$ Z, with the following properties:

1.   ... $V_2 \subset V_1 \subset V_0 \subset V_{-1} \subset V_{-2}$ ...;

2. s(t) $\in V_k$ $\Leftrightarrow$ s(2^k t) $\in V_0$,

3. s(t) $\in V_k$ $\Leftrightarrow$ s(t+1) $\in V_k$

4. $\bigcup\limits_{j=-\infty}^{\infty} V_j$ is dense in L^2 (R) and $\bigcap\limits_{j=-\infty}^{\infty} V_j = \{0\}$,

5. A scaling function $\phi \in V_0$, with a non vanishing integral exists such that the set of $\{\phi(t-l) \mid l \in Z\}$ is an orthonormal basis for V_0, then there exist ψ such that

$$P_{V(k-2)} S = P_{V(k)} S + \sum_{k \in Z} \langle S, \psi_{j,k} \rangle \psi_{k,j} \qquad (8)$$

holds (Daubechies, 1992).

Some of these properties are more of a technical nature. The essential properties are (2) which expresses the fact that all spaces of an MRA are scaled versions of the base space V_0, and (5) which implies that ϕ and ψ should be in a complementary relationship. Since $\phi \in V_0 \subset V_{-1}$ and the $\phi_{-1,l}(t) = 2^{1/2} \phi (2t-l)$ is an orthonormal basis for V_{-1}, there exist $\alpha_l = 2^{1/2} \langle \phi, \phi_{-1,l} \rangle$ so that $\phi(t) = \Sigma_l \phi (2t-l)$. This leads to the relation between ϕ and ψ, $\psi(t) = \Sigma_l (-1)^l \alpha_{-l+1} \phi (2t-l)$ (Daubechies, 1992). The space V_0, itself is spanned by shifted versions of the so-called scaling function ϕ.

To understand the MRA concept the Haar function is convenient. The Haar scaling function is defined as $\phi(t) = 1$ for $0 < t < 1$, $\phi(t) = 0$ otherwise. Then there exists a function ψ and a family ψ_{kj} defined by:

$$\psi_{k,j}(t) = 2^{-\frac{k}{2}}\psi(2^{-k}t - j)$$

(9)

For k fixed, the ψ_j's are orthonormal bases (they never overlap) of the orthogonal complement W_k of V_k in V_{k-1}. In Figures 1a and 1b the Haar scaling wavelet and the Haar analyzing function are shown.
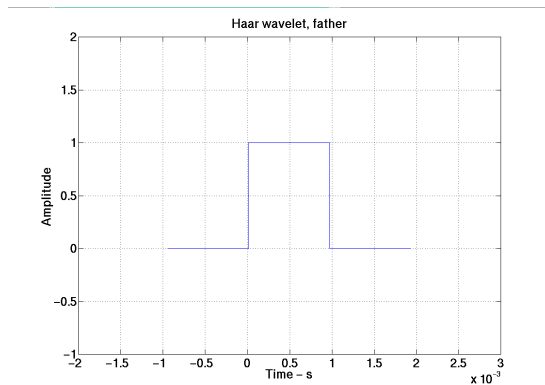
Figure 1a. Haar scaling function or father wavelet.
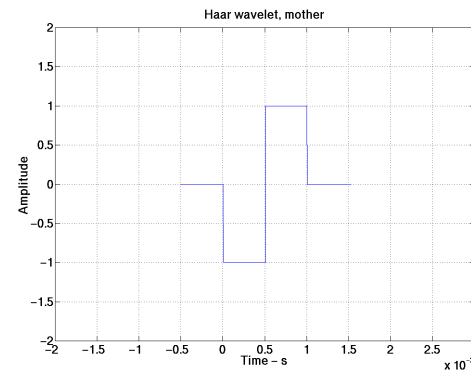
Figure 1b. Haar analyzing function or mother wavelet.

The formula (9), represents a scaled version the of mother wavelet $\psi(t)$. The $\psi_{k,j}(t)$ is a family of wavelet functions generated from the mother wavelet through dilatation determined by the parameter k (*a* in the continuous case) which governs frequency and shift controlled by the parameter j which determines translation (*b* in the continuous case). For any scale 2^{-k}, $\{\psi_{k,j}(t)\}_{k \in Z}$ is an orthonormal basis of W_k. For all scales, $\{\psi_{k,j}(t)\}_{k \in Z}$ is an orthonormal basis of $L^2(R)$ (Mallat, 1999).

Similarly, $\phi_{k,j}(t)$, represent the scaling functions. The family $\{\phi_{k,j}(t)\}_{k \in Z}$ is an orthonormal basis of V_k, (Mallat, 1997).

The functions $\phi(t)$ and $\psi(t)$ are used to measure the signal's local behaviour, that is: the scaling functions $\phi(t)$ and analyzing wavelets $\psi(t)$ are localized in both time and frequency. All the functions that are used are the dilated (or compressed) and shifted versions of the mother wavelet and scaling function. In addition, $\phi(t)$ should be consistent with the averaging interpretation, that is,

$$\int \phi(t)dt = 1$$

(10)

and the analyzing wavelet should be consistent with the differencing interpretation,

$$\int \psi(t)dt = 0$$

$$\qquad (11)$$

($\psi(t)$ is a function of zero mean). These properties can be observed in Figures 1a, and 1b of the Haar wavelets. There are infinitely many function families that satisfy these conditions and can be used as a wavelet basis. The selection of a particular basis is a major and difficult decision in a practical wavelet application.

Using the MRA concept, the DWT can be implemented by high- and low-pass filters that successively decompose the input signal by dyadic downsampling (decimated) convolutions (Mallat, 1999). An arbitrary signal can be represented in such way by the formula:

$$s(t) = \sum_j c_j^{(k)} \phi_j^{(k)}(t) + \sum_k \sum_j d_j^{(k)} \psi_j^{(k)}(t)$$

$$\qquad (12)$$

For k (level of decomposition) fixed:

$$c_j^{(k)} = \langle s, \phi_{k,j} \rangle = \sum_{l \in Z} h_{l-2j} \langle s, \phi_{k-1,l} \rangle = \sum_{l \in Z} h_{l-2j} c_l^{(k-1)}$$

$$\qquad (13)$$

$$d_j^{(k)} = \langle s, \psi_{k,j} \rangle = \sum_{l \in Z} g_{l-2j} \langle s, \phi_{k-1,l} \rangle = \sum_{l \in Z} g_{l-2j} c_l^{(k-1)}$$

$$\qquad (14)$$

If $k = 1$, c_j^1 represent the coefficients of the projection P_1S of s in the space V_1 and d_j^1 represents the coefficients of the projection Q_1S of s in the space W_1 (Keller, 2000).

The variables of g and h represent the filter coefficients of the high, respectively low pass filters. The coefficients $d_j^{(1)}$ are already a final result. They are the coefficients of the wavelet spectrum of s on the scale 1. In order to obtain the wavelet spectrum on the coarser scales 2, 3, 4 and so on, the procedure will be repeated for c_j^1. The two equations (13) and (14) constitute the Mallat's algorithm for the fast computation of the wavelet coefficients of an arbitrary signal s. This procedure can be described using decomposition operators H and G.

$$H : applied \rightarrow c = \{(Hc)_j = \sum_{l \in Z} h_{l-2j} c_l\}$$

$$\qquad (15)$$

$$G : applied \rightarrow c = \{(Gc)_j = \sum_{l \in Z} g_{l-2j} c_l\}$$

$$\qquad (16)$$

This leads to the scheme for the computation of the wavelet spectrum shown in Figure 2. In this example the decomposition goes up to the fourth level, with level 1 containing the highest frequency components.
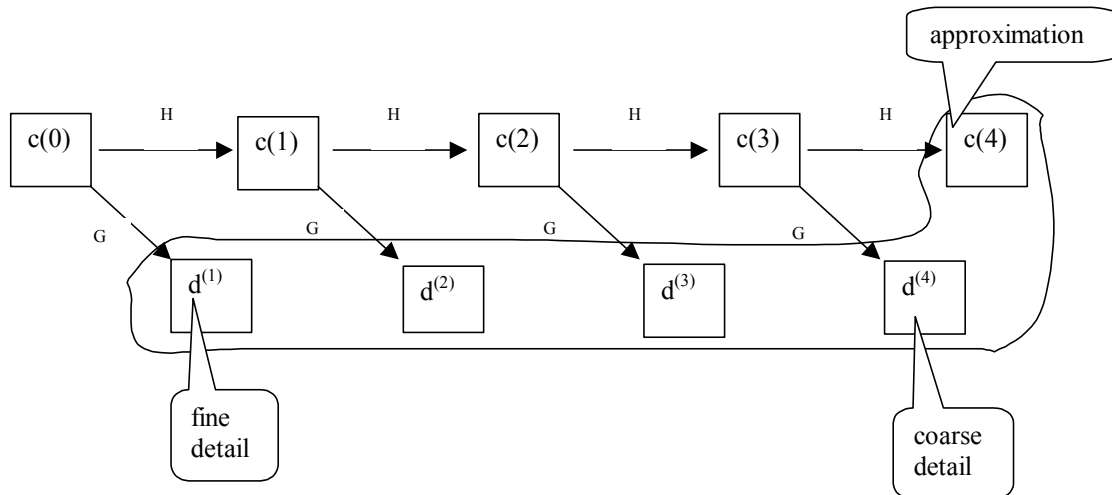
Figure 2. Scheme of the wavelet domain for four levels of decomposition. Those boxes inside the curve form the DWT.

This transform is invertible and the signal is recovered by

$$c_j^{(0)} = \sum_{l \in Z} (c_l^{(1)} h_{2l-j} + d_l^{(1)} g_{2l-j})$$

(17)

METHODOLOGY

The WT is used here to filter seismic data in a time-frequency sense. The primary consideration is how to chose a set of weights to apply them to the WT coefficients. There are infinitely many possible schemes for this. In this paper we investigate the use of a time-domain semblance measure to prescribe the weights.

The filtering was applied to a final stack (Figure 3) of a 2D line from the Blackfoot broad band survey data, recorded in 1995 over the Blackfoot field, owned by PanCanadian (located near Strathmore, Alberta, Township 23, Range 23, West of 4th Meridian). The targets are Glauconitic channels in the Lower Mannville Group of the Lower Cretaceous.
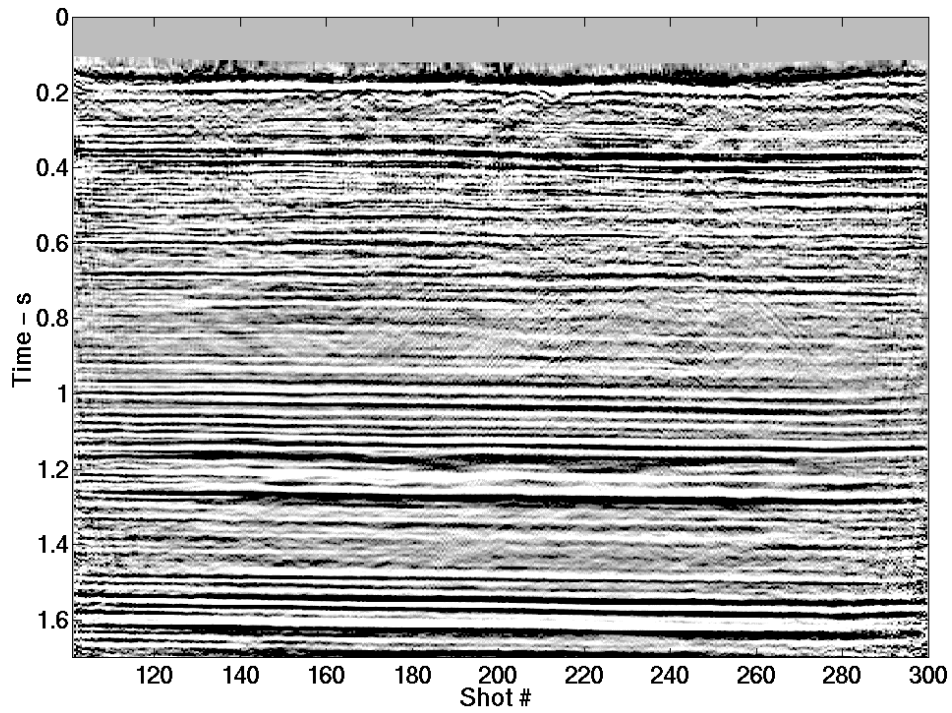
Figure 3. The Blackfoot stacked section.
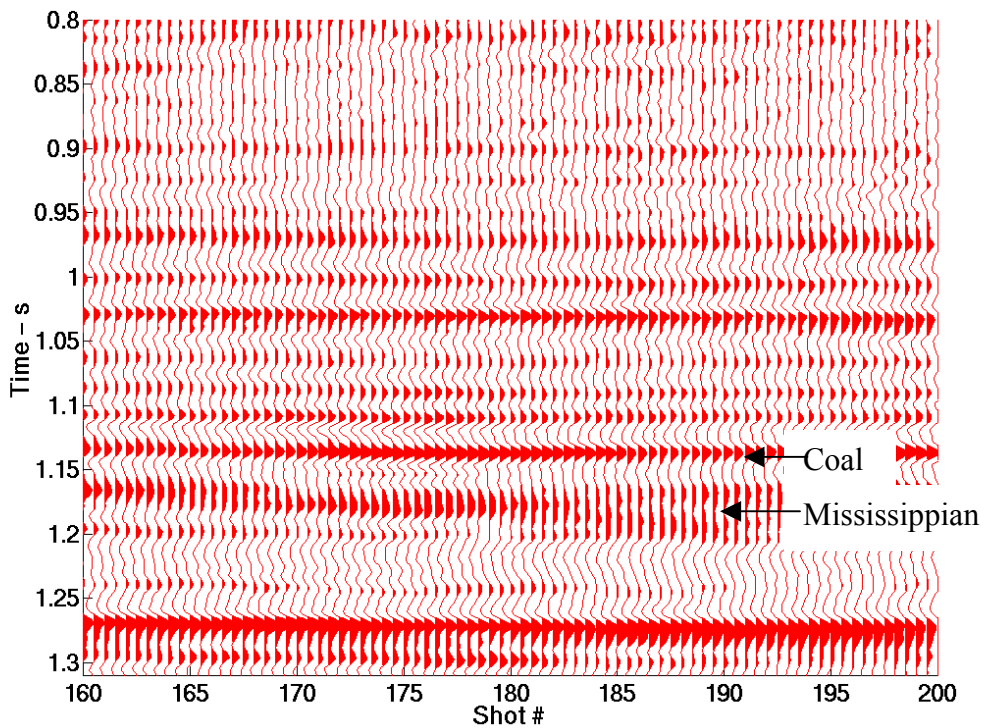
Figure 4. Detail of the Figure 3. The target (Glauconitic channel) extends from the Shot point 170 to 180 between the coal and the Mississippian.

The following procedure was used for WT filtering.

1. Select the desired orthonormal basis (i.e. what wavelet will be used) and a level of decomposition.

2. Calculate multichannel semblance coefficients with smoothing operators of different sizes for the stacked section.

3. Apply the WT to the seismic traces from the stacked section.

4. Apply the WT to the semblance traces. This should extend to the same level of decomposition as for the seismic traces.

5. Weight the wavelet coefficients of the seismic traces with the wavelet coefficients of the semblance traces, that is, multiply their wavelet transforms together.

6. Inverse transform the filtered wavelet coefficients.

7. Apply a time variant spectral whitening (TVSW) operator to the WT filtered stack.

1. Basis selection and decomposition level

The Battle-Lemarie (Daubechies, 1992) wavelet was used in this research because of its good localization in time and frequency. The wavelet transform provides a time-frequency picture and a good localization in both variables is desired. The Haar wavelet described in the representation of the MRA has a poor localization in frequency. Figures 5a and 5b illustrate the amplitude spectrum of the Haar scaling function and the Haar analyzing wavelet.
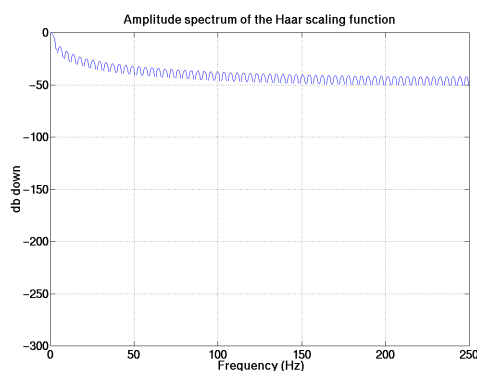
Figure 5a. Haar scaling function in frequency domain.
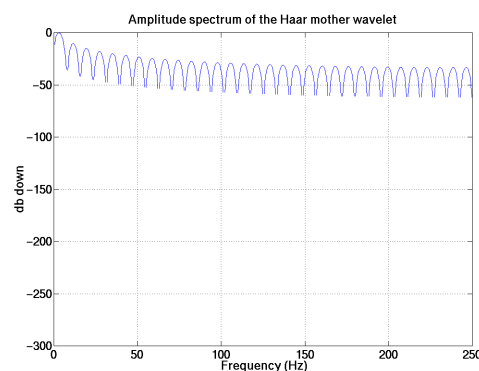
Figure 5b. Haar analyzing function in frequency domain.

The Battle-Lemarie wavelets (in figures 6a, 6b, 6c, and 6d) are spline functions with fast exponential decay in time. In the frequency domain they have a good localization and they have been used in this experiment. According to the Heisenberg uncertainty principle there is a trade off for exponential decay in either time or frequency; one cannot have both (Cohen, 1995). Initially the Battle-Lemarie wavelets have been used in quantum field theory (Daubechies, 1992). Figures 6a - 6d show the representation of the Battle-Lemarie scaling and analyzing functions in time and frequency.
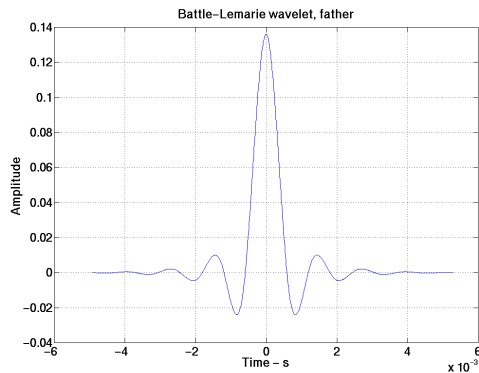
Figure 6a. Battle -Lemarie scaling function.
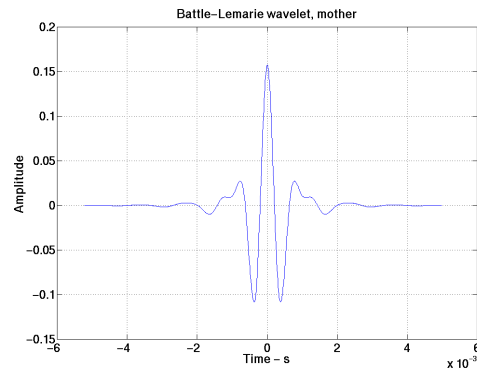
Figure 6b. Battle-Lemarie analyzing function.
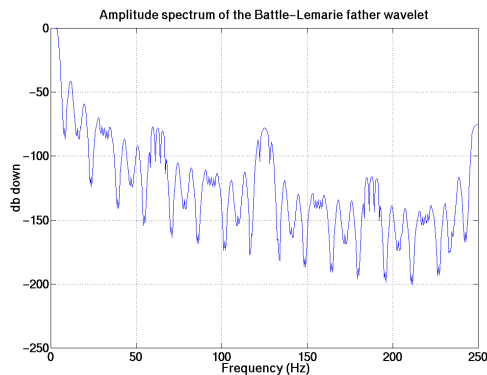
Figure 6c. Battle - Lemarie scaling function in frequency domain.
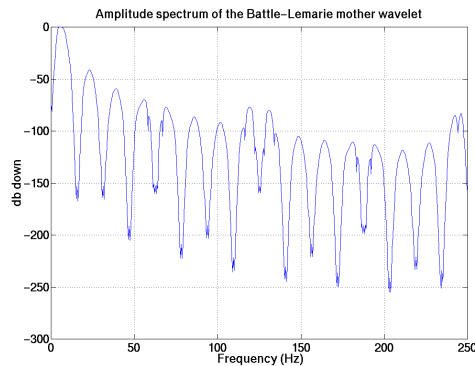
Figure 6d. Battle-Lemarie scaling function in frequency domain.

Using Mallat's algorithm, the level of decomposition was chosen, after considerable experimentation, to be level 2. The stacked section was first decomposed, trace by trace, up to the maximum level, i.e. for a trace of 1500 samples, prior to decomposition a padding to the next power of 2 is mandatory. The maximum level for the padded trace is 11 (2^{11}=2048).

For the level 1 of decomposition, there is 1 set of approximation coefficients and one set of detail coefficients. The highest frequencies of the signal are in the detail part of decomposition whereas the lowest frequencies are in the approximation part of the decomposition. For the level 2 of decomposition, the approximation coefficients

of the level 1 which represents a smoothed version of the original signal downsampled by 2 is again decomposed into another level of detail coefficients which contain the highest frequencies for this level and a set of approximation coefficients. Level 2 implies that the trace in wavelet domain is composed of the detail coefficients of level 1, detail coefficients of level 2 (coarser than 1), and approximation coefficients of level 2, all of them localized in time. The Blackfoot stacked section decomposed for level 2 is illustrated in Figure 7.
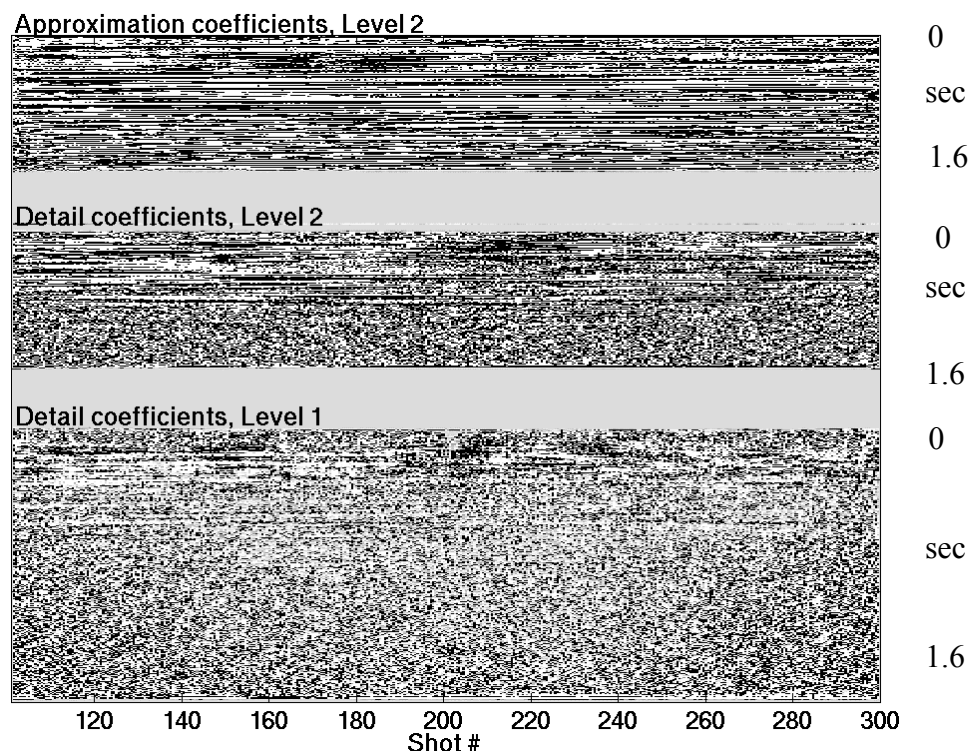
Figure 7. The Blackfoot Stacked section decomposed with Mallat's algorithm to level 2. The approximation and detail coefficients are localized in time.

2. Calculation of Semblance coefficients.

In this study, time-domain semblance coefficients were calculated by:

$$\sigma(x,t) = \frac{1}{\Delta} \frac{[S \bullet a]^2}{S^2 \bullet a}(x,t) ,$$

(18)

where a is a small averaging function, S is the seismic data matrix, Δ is a normalizing constant that depends on a, and $\bullet$ denotes a 2D convolution. In this study, a was a 2D boxcar n traces wide and N samples high.

Currently, coherence measurements are used to detect stratigraphic features and faults and are one of the most important properties of seismic reflection data (Bahorich and Farmer, 1994). Among the formulations that exist for obtaining coherence estimates are cross correlation, semblance, and eigendecomposition of the

data covariance matrix (Gersztenkorn and Marfurt, 1999). In the Blackfoot experiment a semblance algorithm was used. The semblance, as a measure of multichannel coherence can be calculated using different sizes of an operator. An operator higher than 31 samples (15 ms) in the case of the Blackfoot data will blur stratigraphy associated with both deeper and shallower times about the zone of interest. Of the same importance is the width of the semblance operator for the lateral extent of the interest zones. In the case of Blackfoot data, an operator wider than 25 traces will also smear the lateral extent of the zone of interest (i.e. the Glauconitic incised valleys). The semblance operators with good results in this experiment are: 9x3, 3x9, and 5x15.

3. Apply the WT to the seismic traces from the stacked section

The wavelet transform based on Mallat's algorithm was performed on the stacked section to the second level of decomposition. The stacked section in the wavelet domain is illustrated in Figure 7. In this decomposition the Battle-Lemarie wavelet illustrated in Figures 6 was used. The WT was applied to the stacked section or to the whitened stacked section.

4. Apply the WT to the semblance traces

The semblance parameters calculated for different operators shown in step 2 were decomposed in the same way as the stacked section, with the same wavelet, and to the same level of decomposition, respectively 2.

5. Weight the wavelet coefficients of the seismic traces with the wavelet coefficients of the semblance traces.

In the wavelet domain the wavelet coefficients of the stacked section and the wavelet coefficients of the semblance parameters were multiplied. Thus, a decomposition like that of Figure 7 was also performed on the semblance measures (in step #4), then, the two matrices of the wavelet coefficients are multiplied together in a point by point fashion. The resulting matrix of weighted coefficients is the wavelet transform of the filtered data. The steps #4 and #5 were performed for different sizes of the semblance operator (9x3,3x9,and 5x15).

6. Inverse transform the filtered wavelet coefficients.

The inverse transform of the wavelet coefficients of the stacked section weighted by the wavelet coefficients of the semblance parameters was performed. The stacked sections resulted for different sizes of the semblance operators are illustrated in the Figures (8 – 33) and explained in the chapter Discussion of results.

7. Apply a time variant spectral whitening (TVSW) operator to the WT filtered stack.

A TVSW operator was applied to the input data and to the filtered results because it equalizes the Fourier spectrum and therefore, the resolution. The lowest frequency whitened was 5 Hz and the highest 90 Hz. The spectral whitening operator is composed of a set of Gaussian filters. The length of the AGC operator was 0.8 seconds and on every trace 10 Gaussian slices were applied. The TVSW operator was applied a second time for the cases were the WT filtering was performed on the already whitened section.

DISCUSSION OF RESULTS

Figure 8 illustrates the Blackfoot stacked section after the TVSW was applied. Figure 9 represents a detail over the zone of interest in wiggle trace mode. Figures 3 (the original data), 4 (detail of Figure 3), 8, and 9 serve as references in this study.

In Figure 10, a semblance operator of 9x3 served in filtering the data. The stacked section preserves the major reflectors and the unconformity of the Mississippian is better represented than in Figure 3. In detail (Figure 11), it can be observed that a lot of non-coherent noise has been removed, but the major events are very well preserved. The valley of the Glauconitic channel can be distinguished between the shot-points 170 – 180. Figure 12 illustrates the Blackfoot WT filtered section after the TVSW was applied. In detail (Figure 13), it can be observed that the section gained resolution and this time the limits of the channel are very well defined.

The WT filter was also applied to the whitened stacked section. Figure 14 illustrates the stacked section previously whitened and secondly WT filtered. The major events are preserved and there are many similarities with the stacked section in Figure 10. The major limits are very well preserved and the whole character of the section is the same as in Figure 10. After TVSW and WT filter were applied to the data, a second whitening was performed to regain the resolution. From Figure 16 it can be observed that the resolution is boosted and the Glauconitic channel, the Mississippian unconformity and the coal layer above the channel are very well delineated. Comparing Figures 9, 13 , and 17 the details are better enlightened after the WT filter was applied.

The second semblance operator used was a 3x9 boxcar. Figure 18 shows similarities with Figure 10 and 14. The major events have been preserved and the non-coherent noise has been suppressed. The TVSW was applied to the section and the resolution has been improved. Comparing Figures 21 and 9, the details in the WT filtered section (21) are better delineated. The lateral extent of the channel is much better illustrated in Figures 21 (3x9 semblance operator) and 13 (9x3 semblance operator) than in Figure 9.

As in the case of the WT filter with a 9x3 semblance operator, the WT filter with a 3x9 semblance operator has also been applied to the whitened section in Figure 22. The major events has been preserved and enlightened. To increase the resolution the

TVSW filter has been applied second time, after the WT filtering. Figure 24 and the detail in the wiggle trace mode (Figure 25) can be compared to Figures 8, 9, 16 and 17. For the 3x9 operator used in WT filtering, as in the case of the 9x3, described above, it can be observed that in either case, applied directly to the stacked section followed by a whitening, of the data, or applied to the whitened section, followed by another whitening of the data, the lateral and vertical extents of the subtle features in the section are better delineated.

The results of the WT filter that uses a 5x15 semblance operator are the final test in this study. In Figure 26, the stacked section preserves the major reflectors and the unconformity of the Mississippian is again, better represented than in Figure 3. In detail (Figure 27), it can be observed that a lot of non-coherent noise has been attenuated, but the major events are very well preserved. The valley of the Glauconitic channel can be distinguished between the shot-points 170 – 180. Figure 29 illustrates the Blackfoot stacked section after the TVSW was applied. In detail (Figure 29), it can be observed that the section gained additional resolution and this time the lateral and vertical extend of the channel are very well delineated. Figure 29 can be compared to Figures 9, 13 and 21. There are some differences between Figures 13, 21 and 29, due to the size of the boxcar used for calculating the semblance.

The WT filter (with the 5x15 semblance operator) was also applied to the whitened stacked section. Figure 30, illustrates the stacked section previously whitened and secondly WT filtered. The major events are preserved and there are many similarities with the stacked section in Figure 26. The major limits are very well preserved and the whole character of the section is the same as in Figure 26. A second whitening was performed to increase the resolution. From Figure 32 it can be observed that the resolution is increased and the Glauconitic channel, the Mississippian unconformity and the coal layer above the channel are very well delineated. but slightly different than in the cases of other semblance operators used in WT filtering (compare Figures 9 as the reference, with Figures 17, 25 and 33).

CONCLUSIONS

A new filtering technique has been tested. This method is based on wavelet transform and semblance measurements on a stacked section. The total resolution seems to be improved as a consequence of this technique. Prior to applying the WT filtering by semblance weighting it is essential to eliminate the coherent noise such as multiples and shallow reflections. This technique increases the resolution of subtle stratigraphic features, such as Glauconitic channels.

In the first case the WT filtering technique was applied to the final stack followed by a time variant spectral whitening. In the second case, the spectral whitening was applied before and after the WT filtering. The wiggle trace representations illustrate in detail the effect of the WT filtering on the stacked section. As a result of this method the stacked section appears cleaner with a better coherence for subtle details, filtering the non-coherent energy around them. Comparing the results obtained with different semblance operators (9x3, 3x9,and 5x15) it can be observed that the lateral

coherency increases due to the lateral enlargement of the semblance operator (3, 9 respectively 15).

FUTURE WORK

All of the results in this study need to be migrated. This will help to determine if a true improvement in resolution has been attained.

This method should be developed in more detail and tested on different data such as models and different sets of real data. Models with different Q attenuation factors will be constructed. Secondly, random noise at different signal to noise ratio will be added to the model. The W.T. filter will be compared to other more traditional methods of signal enhancement such as spatial prediction.

The semblance can also be estimated in the wavelet domain, similar to calculating the time-variant F-X spectra in the Fourier domain (Margrave, 1999). A new method of estimating the signal bend can be developed in the wavelet domain. These WT semblance estimates can also be used as filter weights. This WT filter will also be examined for ground roll suppression on shot records. It will be compared with more traditional approaches such as F-K filtering.

ACKNOWLEDGEMENTS

REFERENCES

Bahorich, M.S. and Farmer, S.L., 1995, 3-D seismic discontinuity for faults and stratigraphic features: The coherence cube, 65th Ann. Internat. Mtg., Soc. Expl. Geophys., Expanded Abstracts, 1532-1534.

Chakraborty, A. and Okaya, D., 1994, Application of wavelet transform to seismic data, 64th Ann. Internat. Mtg., Soc. Expl. Geophys., Expanded Abstracts, 725-728.

Cohen, L., 1995, Time-frequency analysis, Prentice Hall Inc.

Chui, C.K., 1992, An introduction to wavelets, Academic Press Inc.

Daubechies, I., 1992, Ten lectures on wavelets, Society for Industrial and Applied Mathematics.

Donoho, P., Ergas, R., and Villasenor, J., 1995, High-performance seismic trace compression, 65th Ann. Internat. Mtg., Soc. Expl. Geophys., Expanded Abstracts, 160-163.

Gersztenkorn, A. and Marfurt, K.J., 1999, Eigenstructure-based coherence computations as an aid to 3-D structural and stratigraphic mapping, Geophysics, 64, 1468-1479.

Keller, W., 2000, Lecture notes on wavelets, Univ. of Stuttgart.

Qian, S. and Chen, D., 1996, Joint time-frequency analysis, Prentice Hall Inc.

Mallat, S., 1999, A wavelet tour of signal processing, Academic Press Inc.

Marfurt, K.J., Kirlin, R.L., Farmer. S.L. and Bahorich, M.S., 1998, 3-D seismic attributes using a semblance-based coherency algorithm, Geophysics, 63, 1150-1165.

Margrave, G.,F., 1999, Seismic signal band estimation by interpretation of f-x spectra, Geophysics, 64, 251 – 260.

Rodriguez, J.M. and Mansar, S., 1996 Analyzing and correcting seismic phases using the wavelet transform, 61st Mtg. Eur. Assoc. Expl Geophys., Extended Abstracts, P187.

Schoepp, A., 1998, Improving Seismic Resolution with Nonstationary Deconvolution, M.Sc. thesis Univ. of Calgary.

EXAMPLES
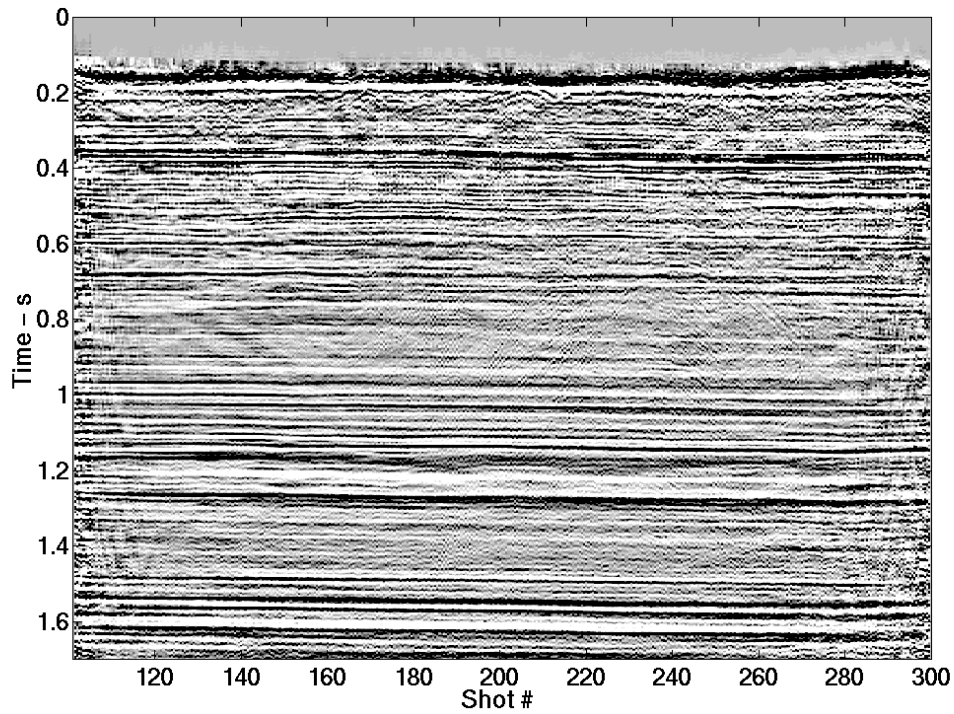
Figure 8. Similar to Figure 3 except that the data has been through TVSW.
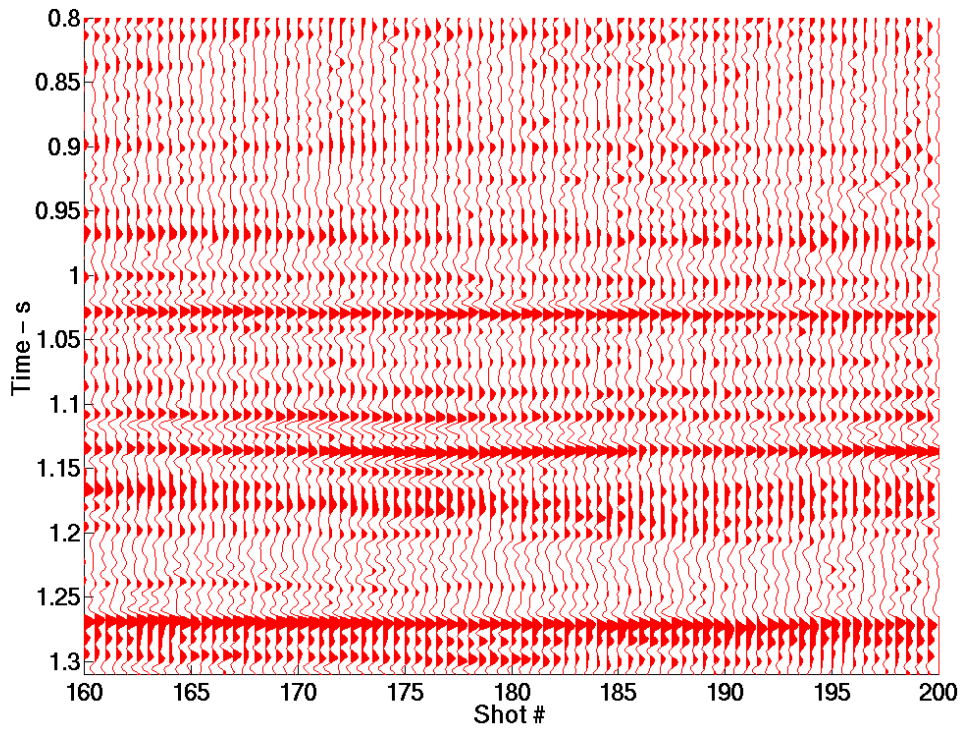
Figure 9. Detail of the Figure 8. (To be compared with Figure 4)
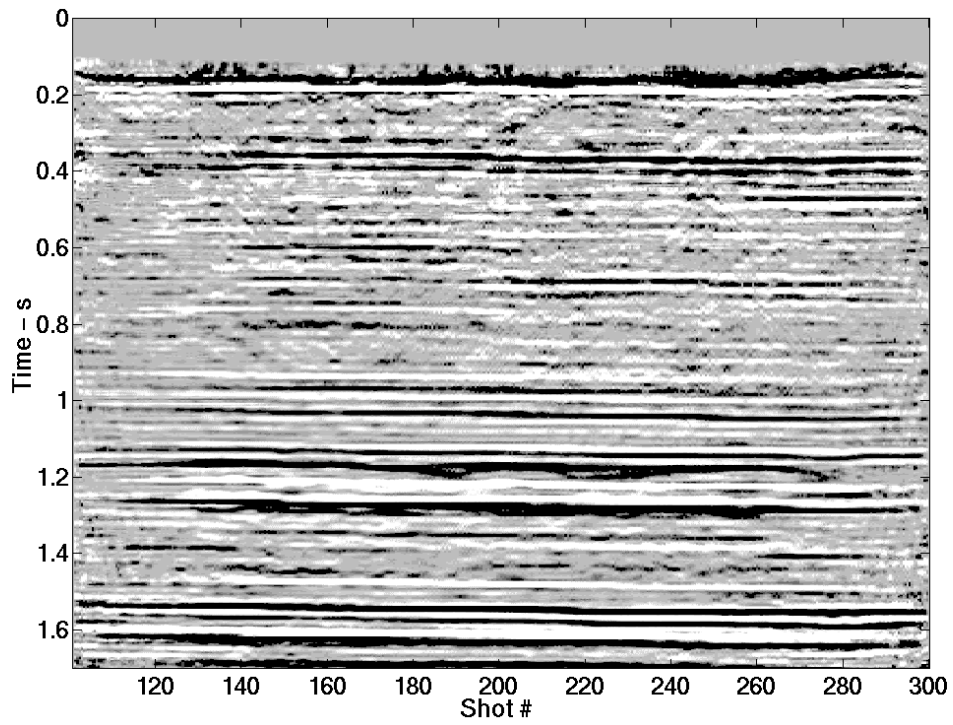
Figure 10. The Blackfoot data, after WT filtering, a 9x3 semblance operator was used. (To be compared with Figure 3)
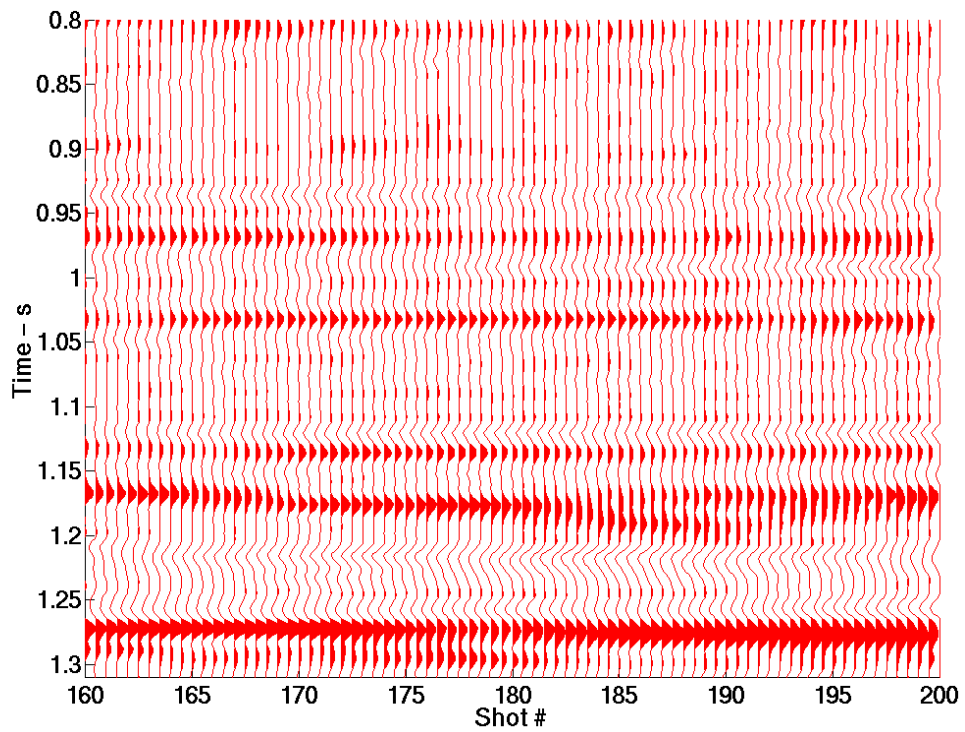

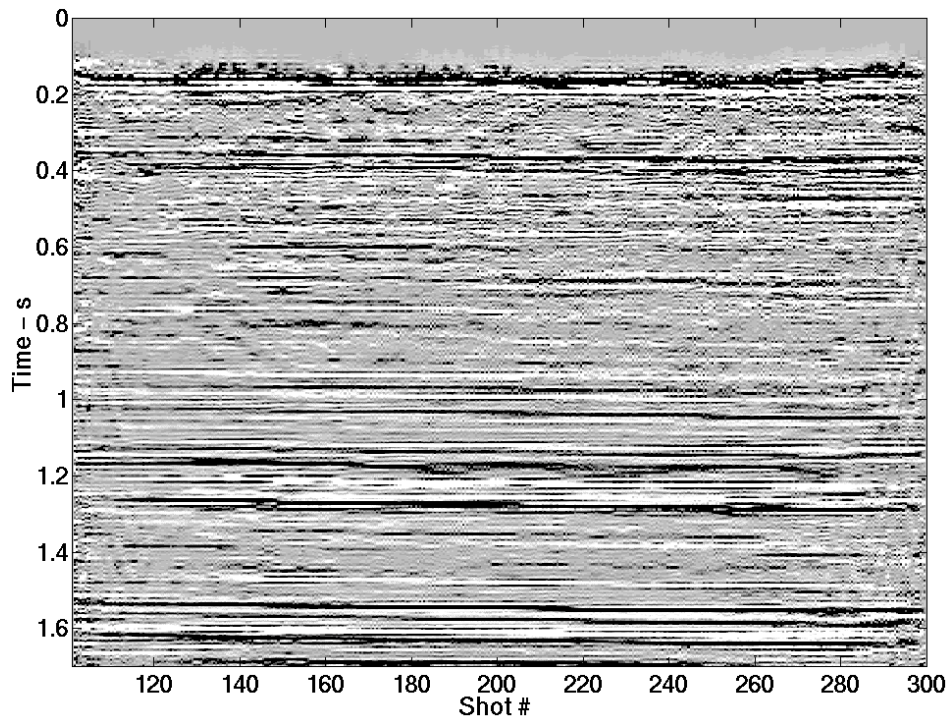Figure 11. Detail of Figure 10. (To be compared with Figure 4)

Figure 12. Similar to Figure 10 (9x3 operator) except that the data has been through TVSW after the WT filtering. (To be compared with Figure 8)
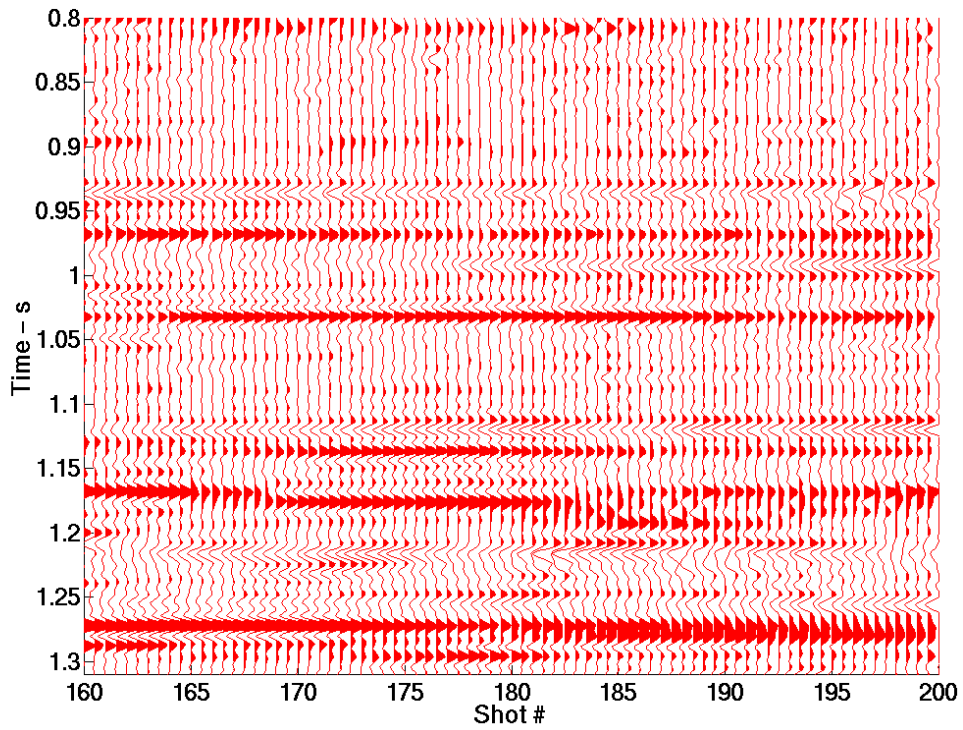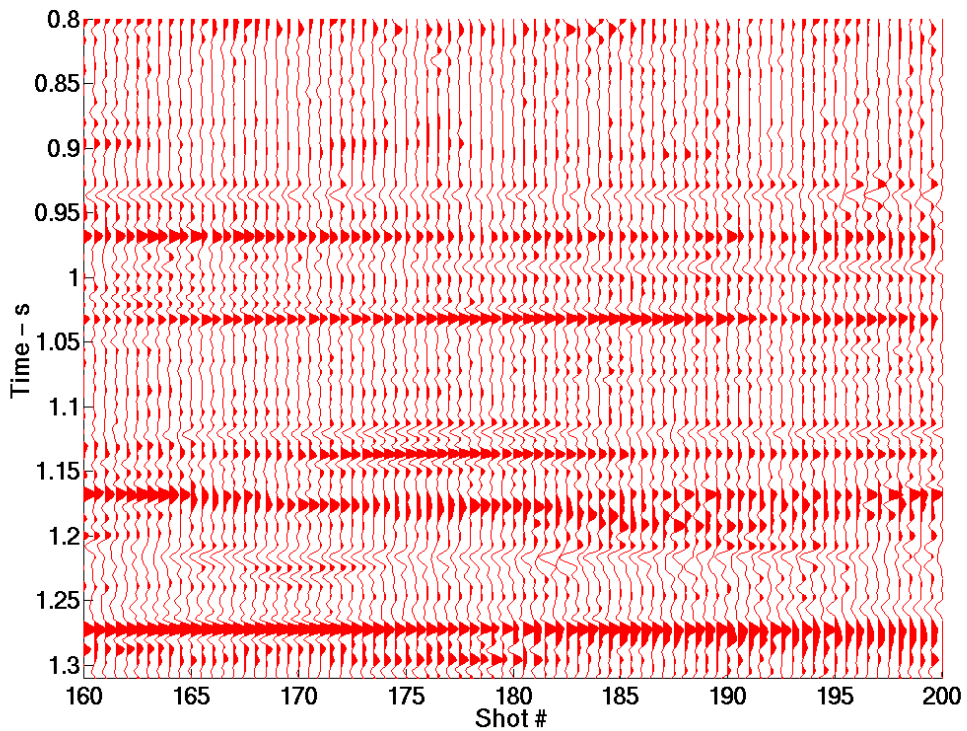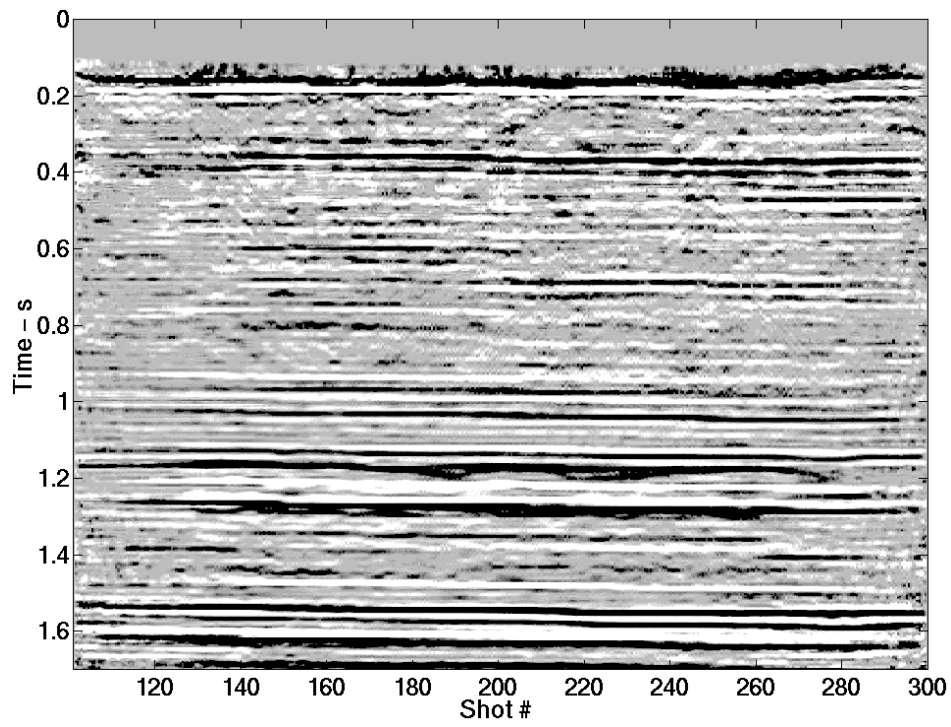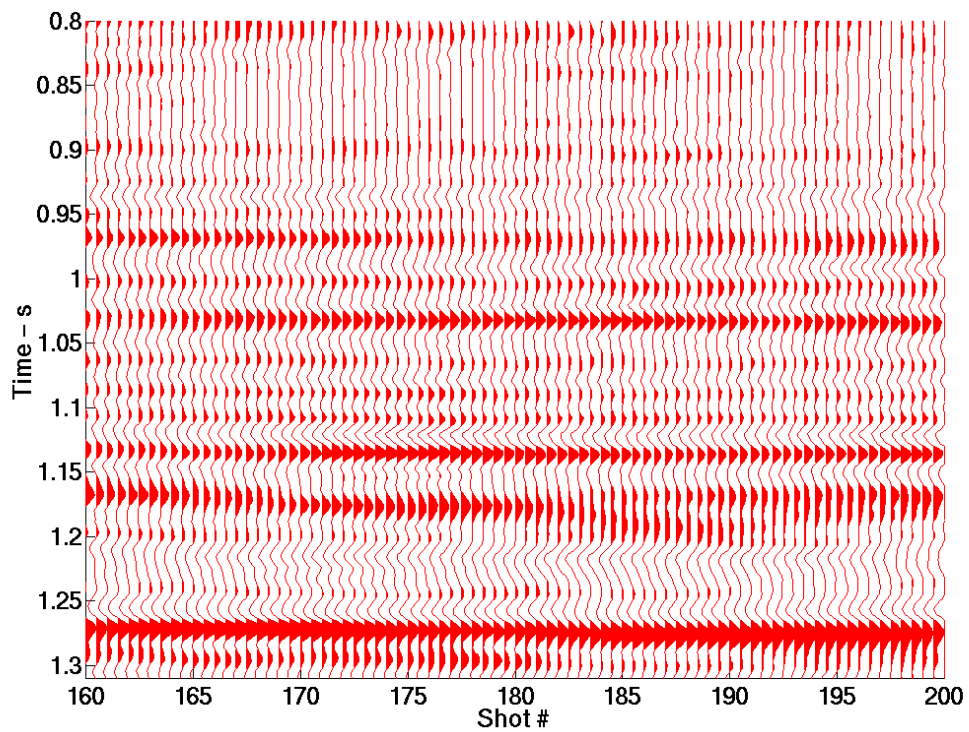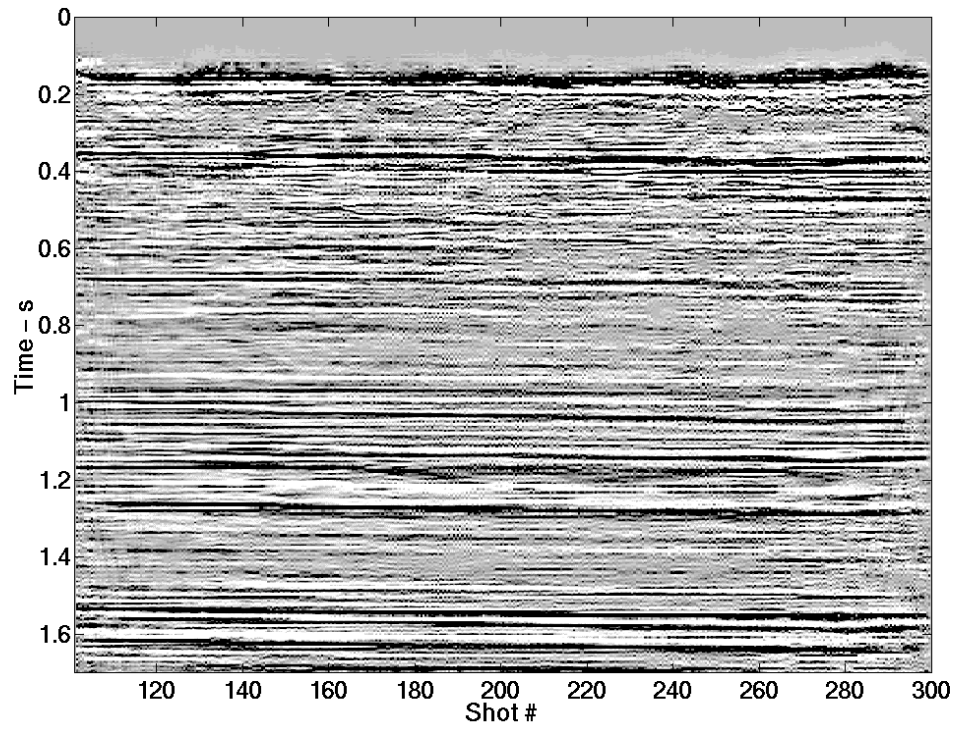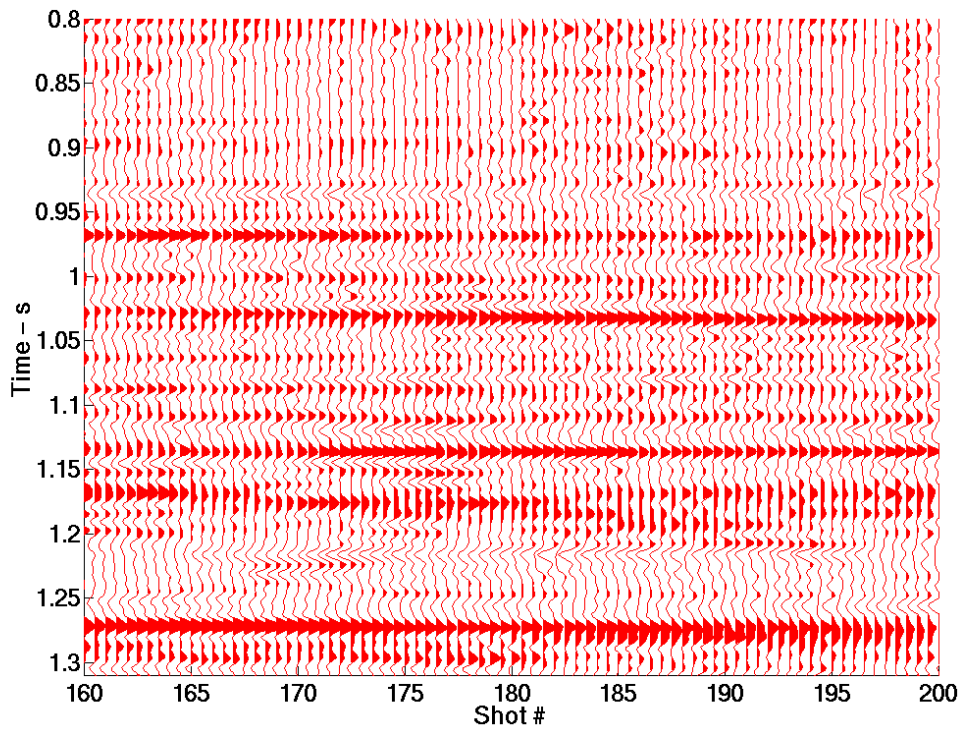

Figure 13. Detail of Figure 12. (To be compared with Figure 9)
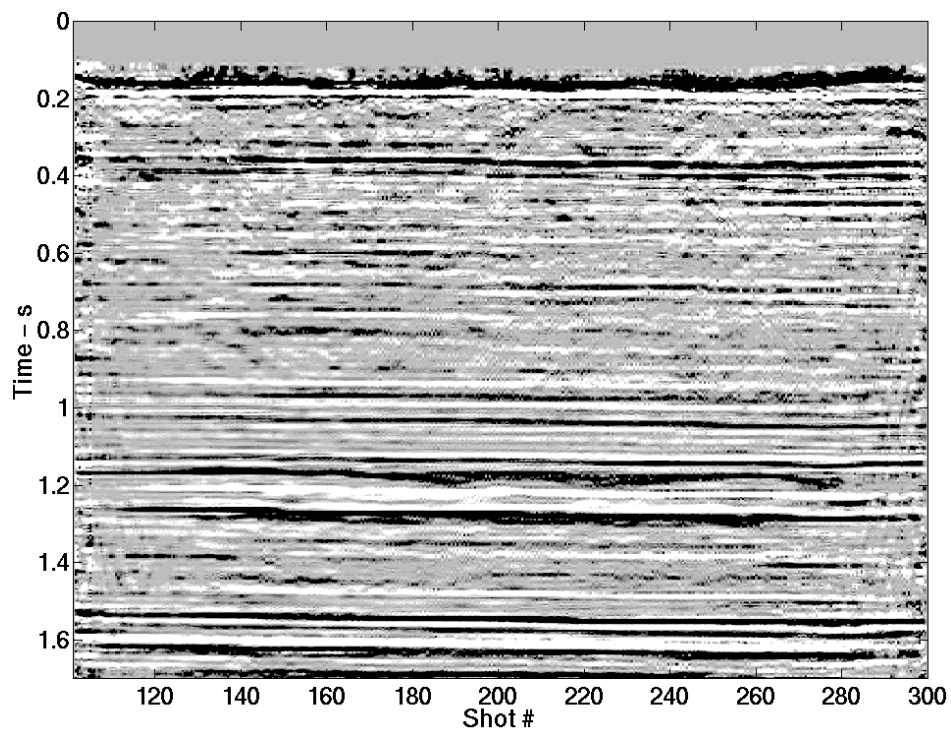
Figure 14. This stacked section was previously whitened and then WT filtered. Semblance operator size = 9x3. (To be compared with Figure 8)
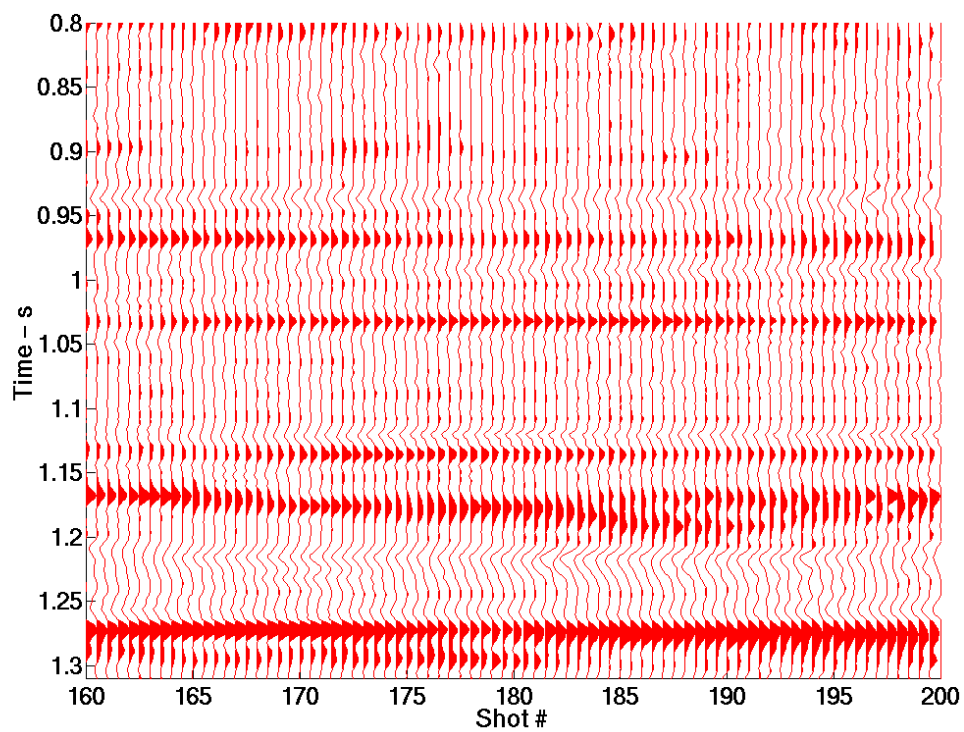
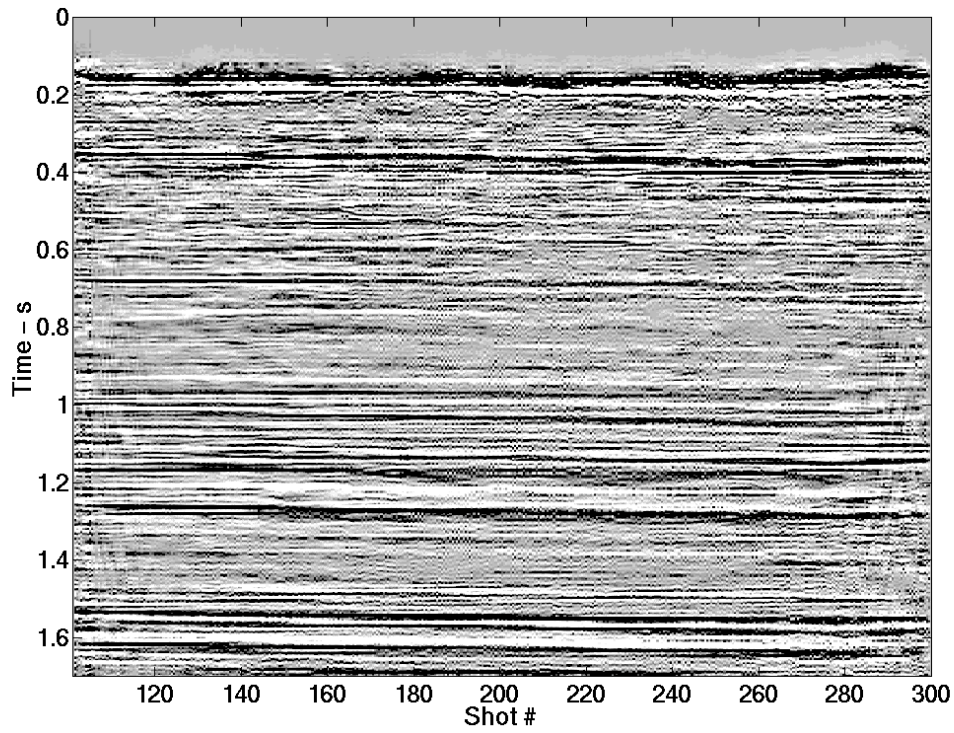Figure 15. Detail of Figure 14. (To be compared with Figure 9)
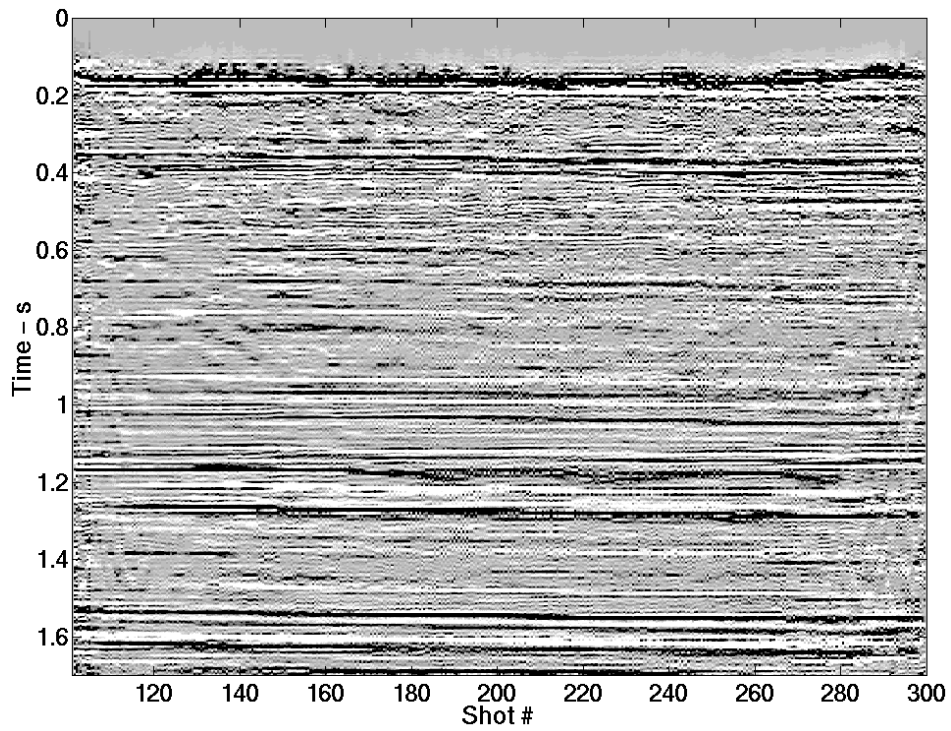
Figure 16. Similar to figure 14. The data has been through TVSW again after WT filtering (Semblance operator, 9x3). (To be compared with Figure 8)
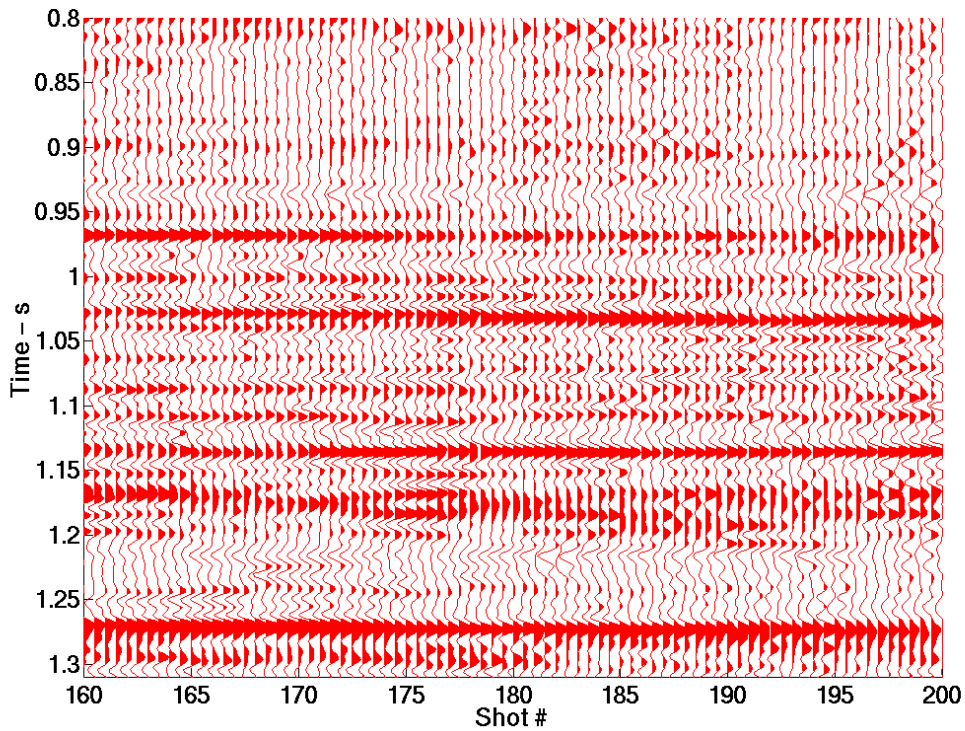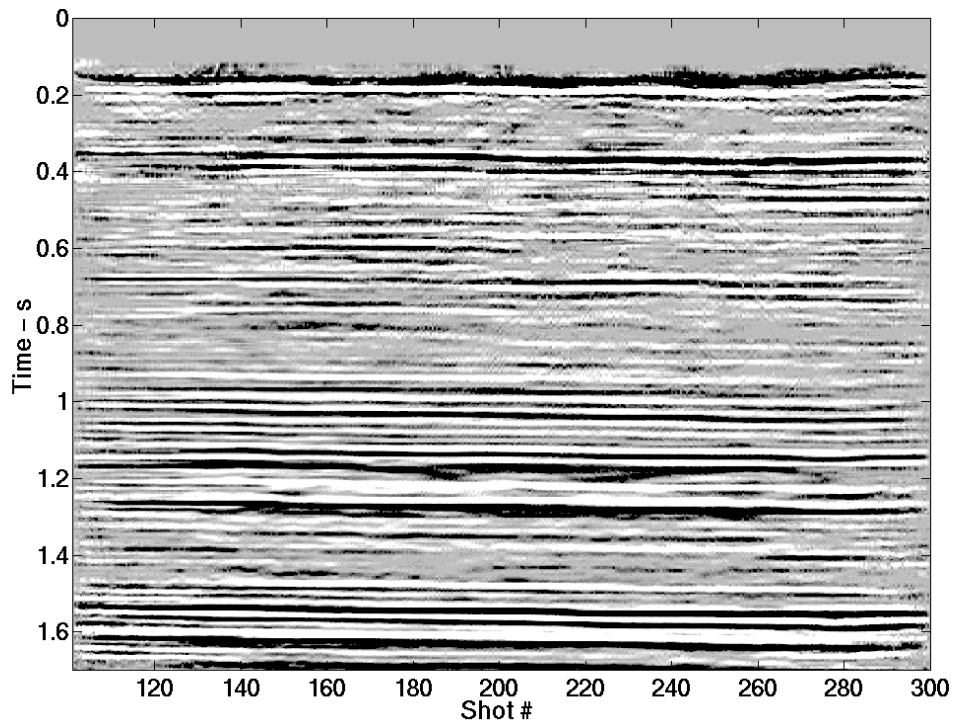

Figure 17. Detail of Figure 16. (To be compared with Figure 9)

Figure 18. The Blackfoot data, after WT filtering, a 3x9 semblance operator was used. (To be compared with Figure 3)

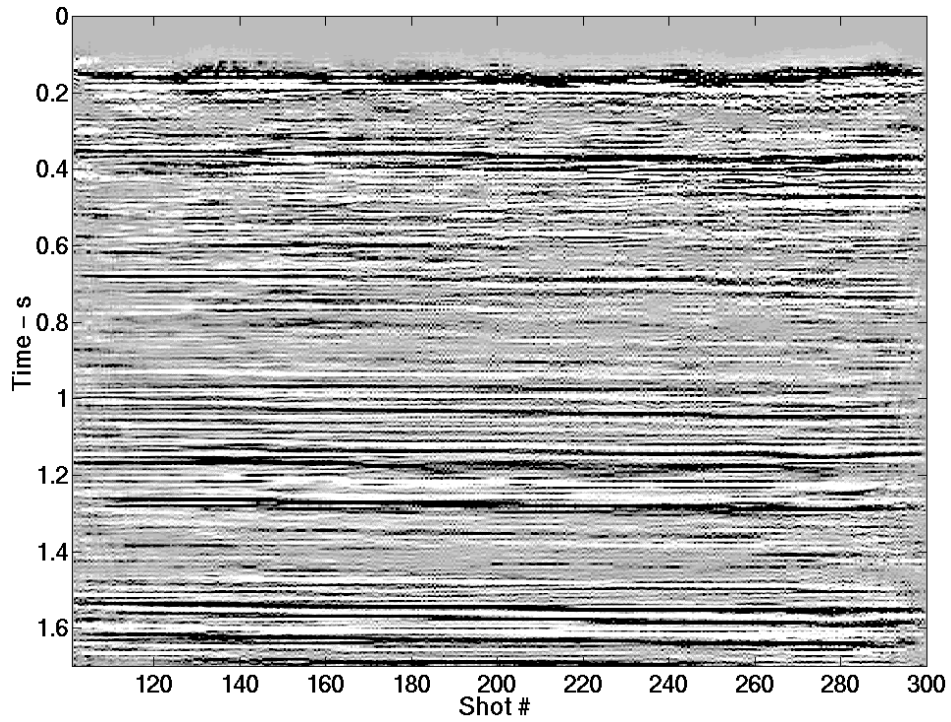Figure 19. Detail of Figure 18. (To be compared with Figures 4 and 11)

Figure 20. Similar to Figure 12 (3x9 operator) except that the data has been through TVSW after the WT filtering. (To be compared with Figures 8 and 16)
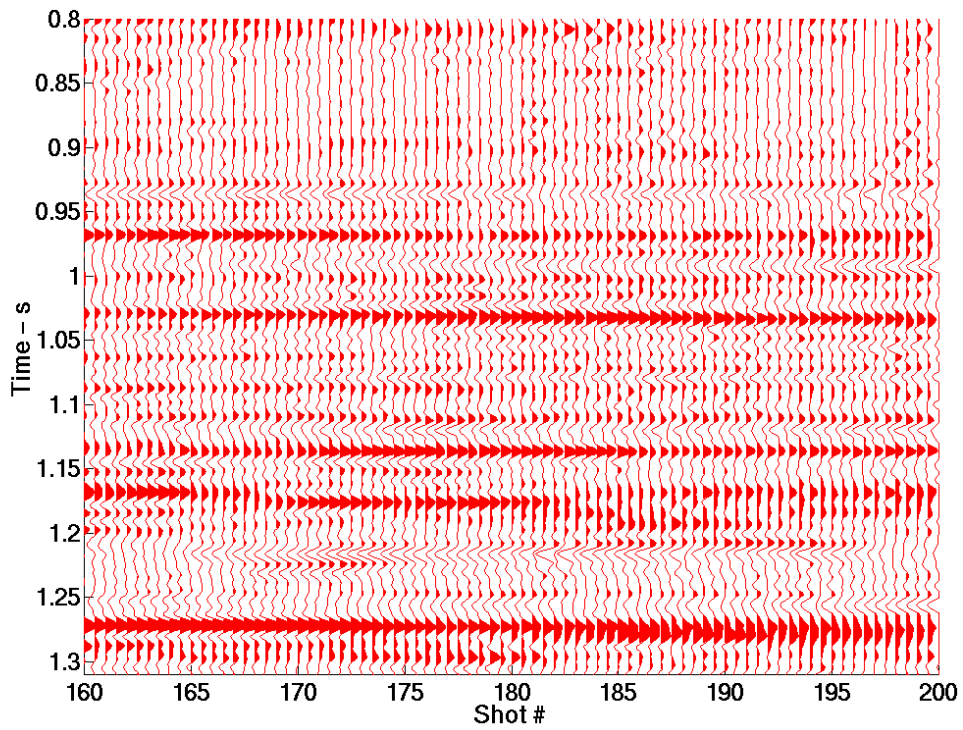

Figure 21. Detail of Figure 20. (To be compared with Figures 9 and 13)
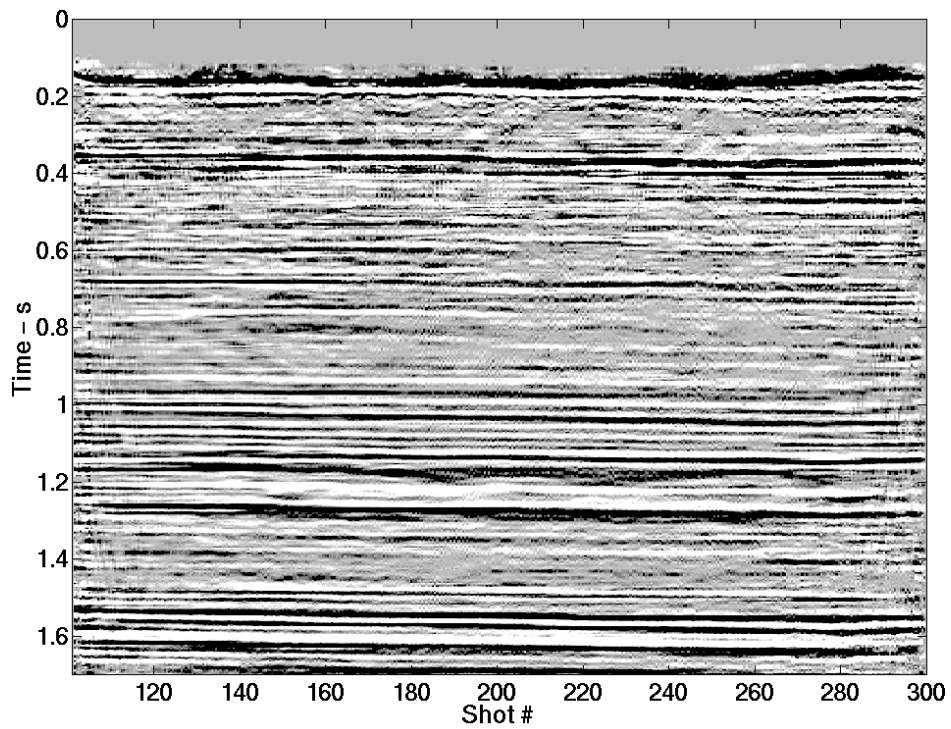
Figure 22. The stacked section was previously whitened and then WT filtered. Semblance operator size 3 x 9. (To be compared with Figures 8 and 16)
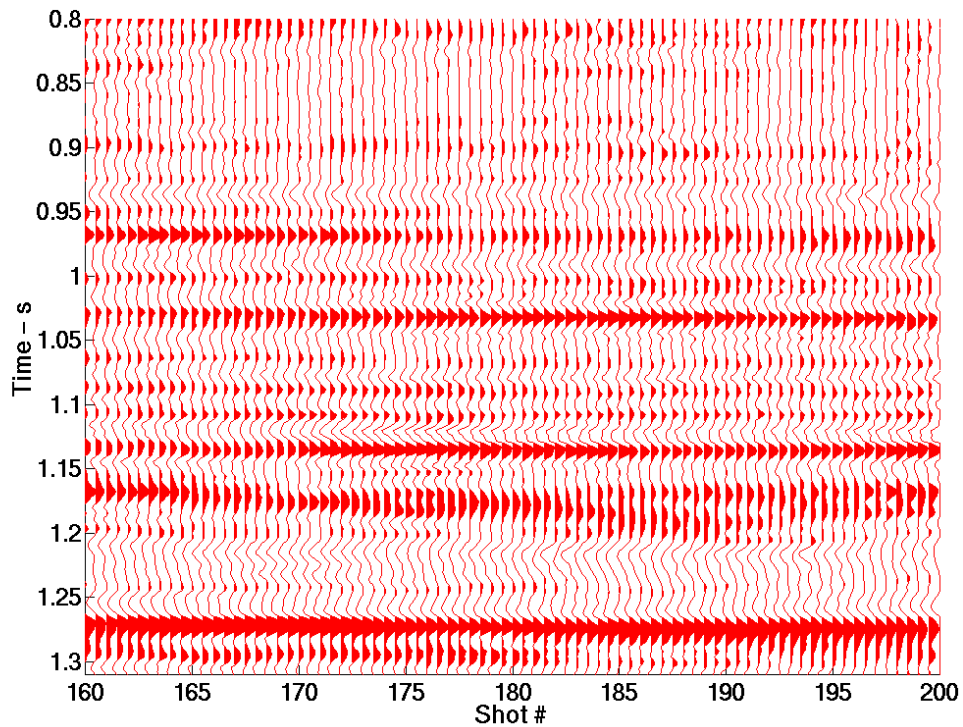
Figure 23. Detail of Figure 22. (To be compared with Figures 9 and 17)

Figure 24. Similar to figure 22. The data has been through TVSW again after WT filtering (Semblance operator, 3x9). (To be compared with Figures 8 and 16)

Figure 25. Detail of Figure 24. (To be compared with Figures 9 and 17)

Figure 26. The Blackfoot data, after WT filtering, a 5x15 semblance operator was used. (To be compared with Figures 3, 10 and 18)
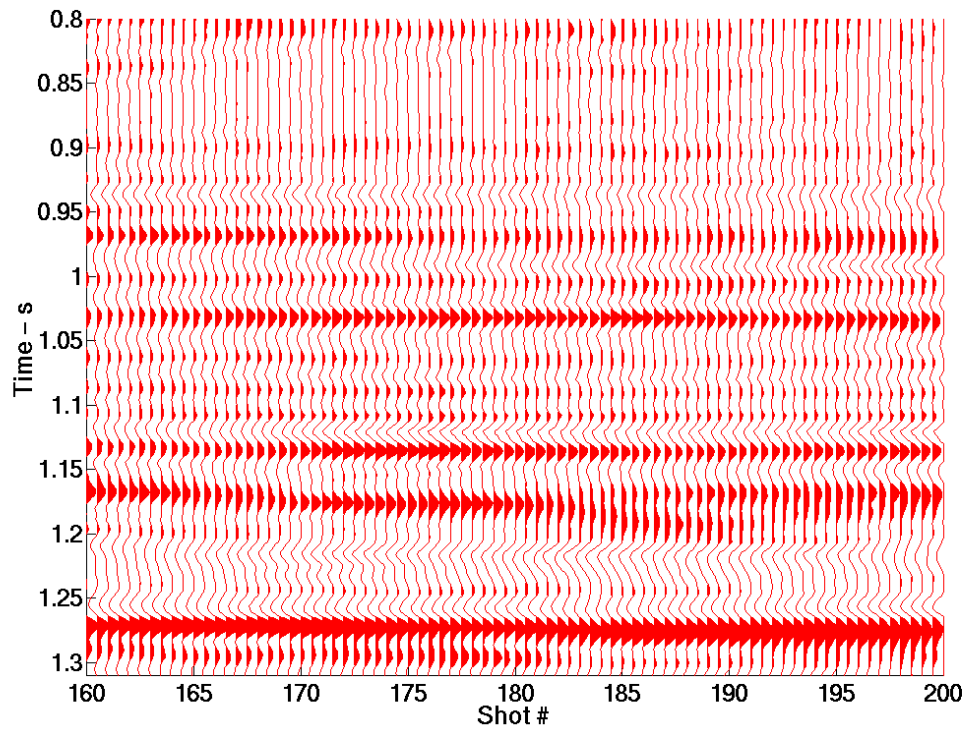
Figure 27. Detail of Figure 26. (To be compared with Figures 4, 11 and 19)

Figure 28. Similar to Figure 23 (5x15 operator) except that the data has been through TVSW after the WT filtering. (To be compared with Figures 8, 12 and 20)

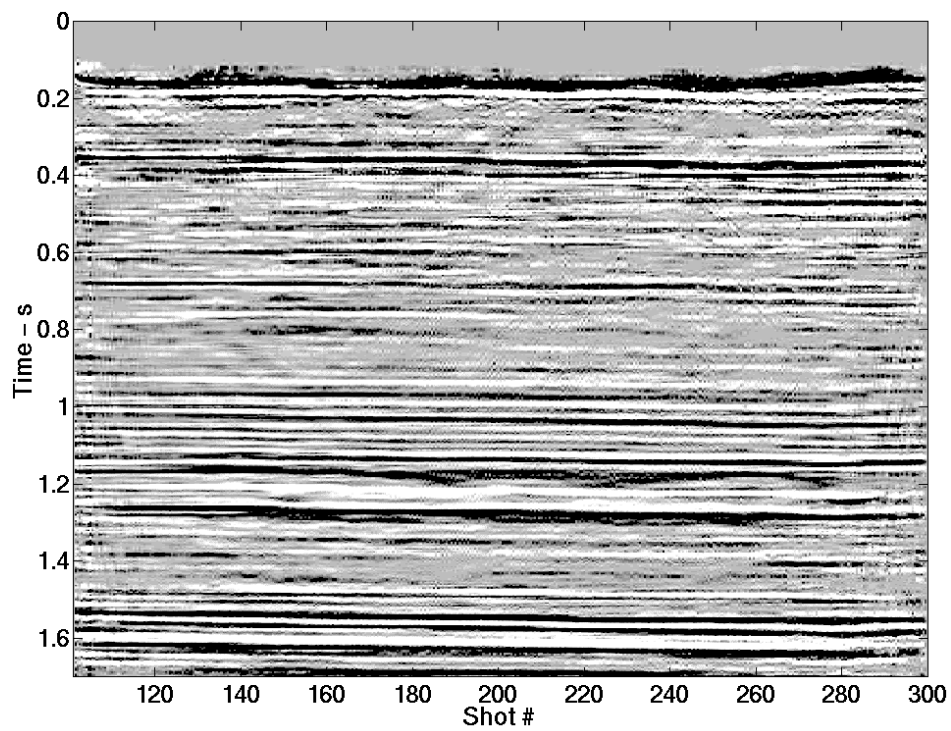Figure 29. Detail of Figure 28. (To be compared with Figures 9, 13 and 21)

Figure 30. The stacked section was previously whitened and then WT filtered. Semblance operator size 5 x15. (To be compared with Figures 8, 14 and 22)
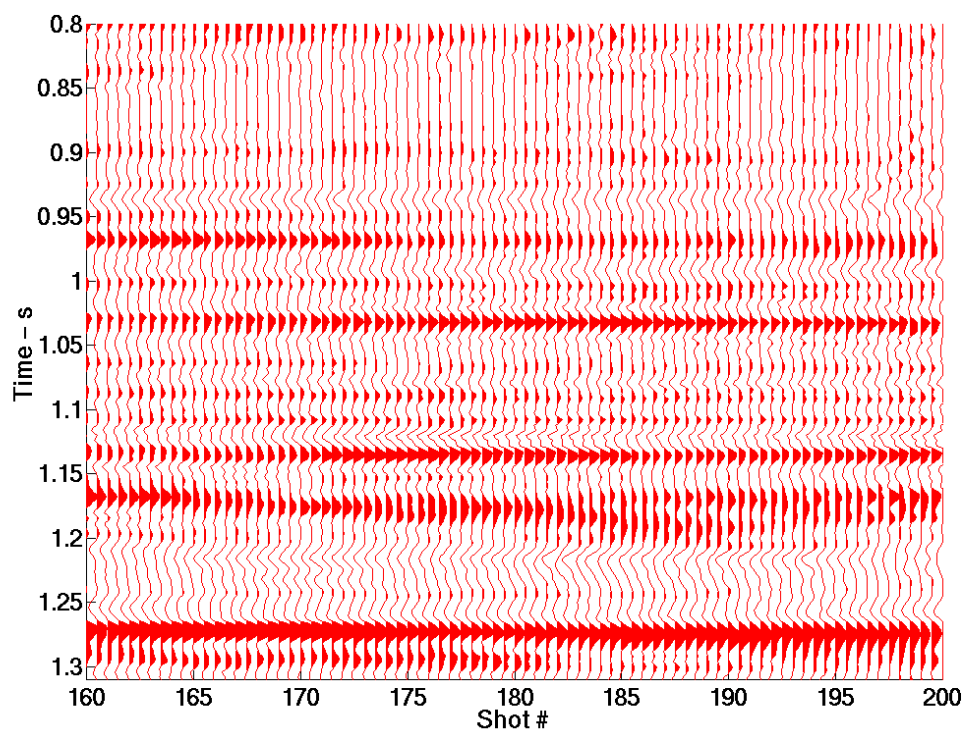

.

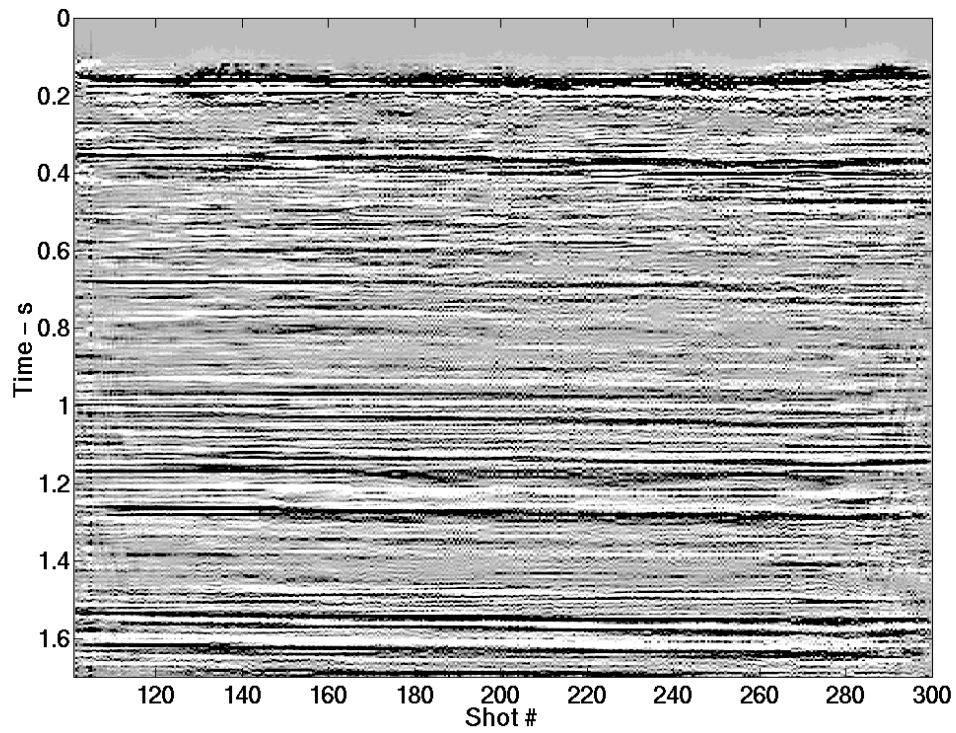Figure 31. Detail of Figure 30. (To be compared with Figures 9, 15 and 23)

Figure32. Similar to figure 30. The data has been through TVSW again after WT filtering (Semblance operator, 5x15). (To be compared with Figures 8, 16 and 24)
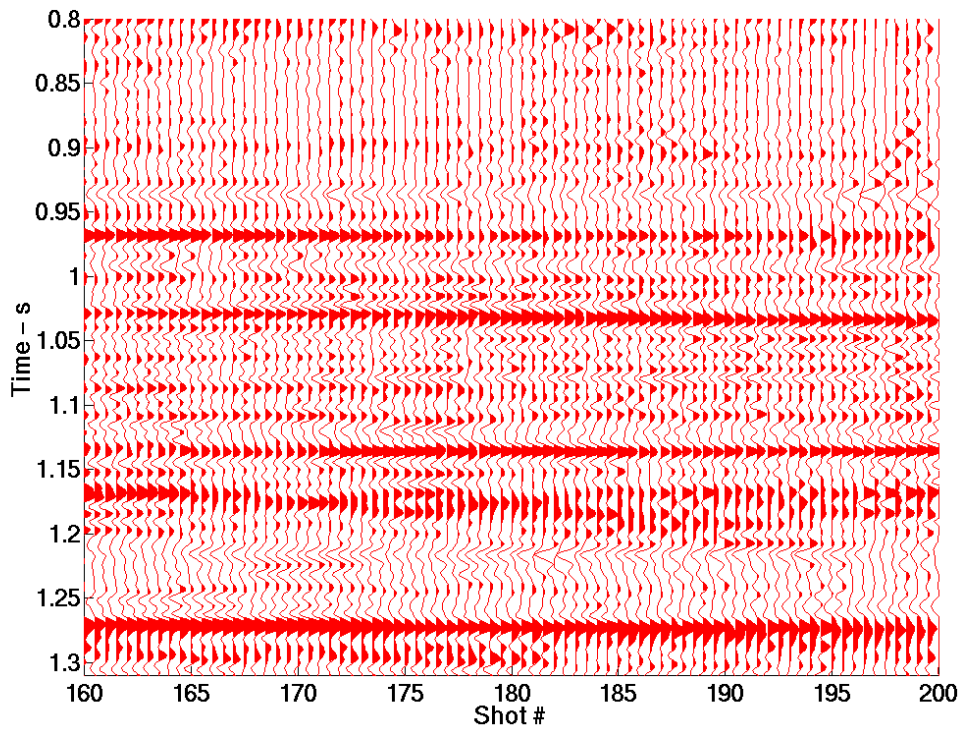

Figure 33. Detail of Figure 32. (To be compared with Figures 9, 17 and 25)